

Computing the Influence Functions of an Adaptive Optics Large Deformable Mirror: the Numerical Method and the Experimental Data

C. Del Vecchio^{*,1}, R. Briguglio¹, M. Xompero¹, A. Riccardi¹, D. Gallieni² and R. Biasi³

¹INAF-OAA, ²ADS International, ³Microgate

*L. Enrico Fermi 5 I-50125 Firenze, Italy, cdelvecchio@arcetri.astro.it

Abstract:

Adaptive Optics units are mounted on many large telescopes, thus enabling diffraction-limited astronomical images through compensation of the effects of atmospheric turbulence. The design of the control system of the Deformable Mirror includes a feed-forward block, aimed for increasing the efficiency of the control loop. Such a block is based on the stiffness matrix of the Deformable Mirror, defined as the force required to move a single actuator while all the others are constrained at zero positions. The mirror shape caused by this force pattern is called Influence Function. This paper discusses the computation methods adopted to calculate the influence functions of the LBT and VLT Deformable Mirrors, grounded in the capabilities of the Comsol/Matlab interactions. The comparison of the Comsol results with the data available from the optical tests shows that the methods analyzed in this paper are suitable for accurately predicting the delicate optomechanics of the Deformable Mirrors.

Keywords: Adaptive Optics, Optomechanics, Influence Function, FEA

1 Introduction

The Adaptive Optics (AO) units implemented on many large telescopes allow to obtain diffraction limited astronomical images by compensating the effects of the atmospheric turbulence. The control system of a typical AO unit, sketched in figure 1, provides the correction of the distorted wavefront deforming the Deformable Mirror (DM) by means of several actuators. The closed-loop response is dramatically increased when a *feed-forward*, open-loop correction is added to the servo system, as dis-

cussed in [2]. This correction is based on the stiffness matrix of the DM, which is operatively defined by arbitrarily displacing one of the DM actuators along the normal to the thin mirror surface, while all the other actuators are constrained at their nominal positions, and calculating all the reaction forces. In the AO terminology, the shape of the DM when poking a single actuator is known as the influence function (IF), whose numerical computation is discussed in this paper. The method adopted to calculate the IF of the concave DM of the Large Binocular Telescope (LBT), described in [6], and of the convex DM of the Very Large Telescope (VLT), described in [1], is based on some Matlab scripts and functions, found on the capabilities of LiveLink for Matlab.

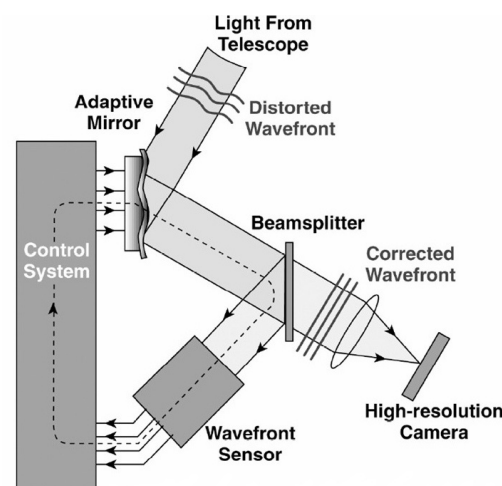


Figure 1: Scheme of an AO control system.

Starting from the optical and physical parameters of the thin mirrors and the geometrical layouts of the actuators, a first script builds the geometry, applies the physics required to solve the problem and sets up the meshes. In fact, the complexity of the actuator geometry (the LBT and the

VLT DMs have 672 and 1170 actuators, respectively) and the accuracy required by the optics when modeling the geometry of the actual glass shell makes the Comsol GUI ineffective. Moreover, as many auxiliary coordinate systems as the number of actuators should be defined in order to properly apply the required constraints. Unfortunately, this large number increases dramatically the data to be stored by Comsol — which, as a matter of fact, makes this choice unworkable. Thereby, an alternative method is carried out: the constraints are implemented via a user-defined interpolation function, whose input is defined by the Matlab algorithm discussed in section 2.2. Finally, a further function runs the computational loop and performs the post-processing of the results, as examined in section 3.

The comparison of the displacements acquired by interferometric analyses and of the the actuator forces derived from electrical measures — such data have been collected during the test runs, as explained in [6] — with the Comsol results shows a good agreement, analyzed in section 4.

2 Static assumptions and simplifications

2.1 The model

	LBT	VLT
R_o	455.5 mm	558 mm
R_i	28 mm	48 mm
t_m	1.6 mm	2.0 mm
R_b	1994.9 mm	4575.30 mm
K_b	0	0
R_f	1974.24 mm	4575.3 mm
K_f	-0.7330	-1.66926
N	672	1170

Table 1: The optical and physical main parameters of the LBT and VLT Zerodur DMs. R_o and R_i designate the physical outer and inner radii, respectively; K_f and K_b the front and back surface conic constants, respectively; R_f and R_b the front and back surface optical radii, respectively; t_m the mean thickness; N the total number of actuators.

*The truss elements are modeled as beam elements with negligible moments of inertia and torsional constant, because of a known Comsol issue about dealing with a large number of trusses

†As no force is applied perpendicularly to the actuator axis, l_p can be arbitrarily chosen.

Starting from the optical parameters listed in table 1, the aspherical and spherical axially symmetric surfaces of both the DMs can be generated in Matlab as $z_f = z_f(r)$ and $z_b = z_b(r)$, with $r = \sqrt{x^2 + y^2}$. Because of the values of table 1, the mean surface $z = (1/2)(z_f + z_b)$ as well as the thickness $t = |z_f - z_b|$ are very accurately fitted by the polynomials $v(r)$ and $q(r)$, respectively, of degree $M = 9$. Moreover, also the angle $\varphi = -\arctan(dz/dr)$, defined in section 2.2, can be accurately approximated by the polynomial $p(r)$ of degree M . Naming \mathbf{V} , \mathbf{P} , and \mathbf{Q} the $M + 1$ coefficients of $v(r)$, $p(r)$, and $q(r)$, respectively, z , t , and φ can be analytically defined in the Comsol Finite Element Model (FEM) according to (1), (2), and (3), respectively. As a consequence, the geometry generation is quite easy and all the relevant variables are available in Comsol.

$$z = \sum_{i=1}^{M+1} V(i)r^{M+1-i} \quad (1)$$

$$\varphi = \sum_{i=1}^{M+1} P(i)r^{M+1-i} \quad (2)$$

$$t = \sum_{i=1}^{M+1} Q(i)r^{M+1-i} \quad (3)$$

Both the VLT and LBT DMs strokes are actuated by magnetic forces, as described in [3], which are applied perpendicularly to the DM by a *puck* built of a magnet and a glass disk glued to it via three glue spots, angularly equispaced at a distance $r_g = 2$ mm from the puck axis — the blue arrow in figure 2. Modeling the full puck with a solid FEM, restrained at the three glue/DM interfaces and loaded by a body force inside the magnet, allows to calculate K_p , the overall stiffness of the puck as $K_p = 112.5 \text{ N} \times \mu\text{m}^{-1}$. As the spot diameters are as small as $\approx 50 \mu\text{m}$, the magnetic forces applied to the Zerodur DM, modeled as a shell, can be approximated by the three trusses* of length $l_p = 10 \text{ mm}$ † perpendicular to the DM surface (pictured in black in figure 2) and the three rigid beams of length $r_g = 2$ mm (pictured in yellow in figure 2). The actual response of the full puck is well approximated by assigning a

null density to the truss and beam elements and by the following two inputs: naming A_p the truss cross sections and E_p its Young's modulus, A_p must satisfy the relationship $K_p = 3E_p A_p / l_p$; the beam elastic and cross section data are chosen in order to define a beam rigidity several orders of magnitude larger than the truss and DM stiffnesses. Finally, the three beam/truss interfaces are restrained along the red and green directions in figure 2, perpendicular to the blue axis, identifying the stroke direction.

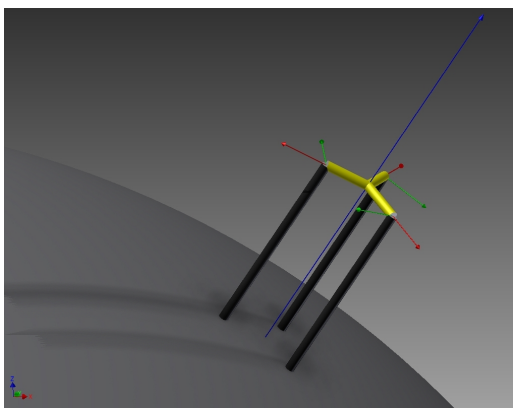


Figure 2: Approximation of the *puck*. See the text for a discussion.

The effects of the central flat membrane, described in [4], placed perpendicularly with respect to z , whose z stiffness is K_m , are simulated by the edge load $(-K_m / (2\pi R_i)) \times (w - 0)$ and the prescribing a null radial and tangential (with respect to the xy plane) displacement of the edges at $r = R_i$.

The VLT and LBT obtained models consist of 32824 triangular elements and 7020 beam elements and 19144 triangular elements and 4032 beam elements, respectively.

2.2 Coordinates functioning

As the actuators axes are perpendicular to the DM surface, the natural manner to properly define displacements and forces within Comsol is the implementation of as many auxiliary coordinate systems as the number of the actuators. Defining φ the angle between the optical axis Z and the normal to the DM at the point $P \equiv (X, Y)$, with $R = \sqrt{X^2 + Y^2}$ and $\theta = \arctan(Y/X)$, the “global-to-local” and “local-to-global” trans-

formation matrices \mathbf{G} and $\mathbf{L} = \mathbf{G}^{-1}$ are defined as in (4) and (5), respectively:

$$\begin{bmatrix} \cos(\varphi) \cos(\theta) & \cos(\varphi) \sin(\theta) & \sin(\varphi) \\ -\sin(\theta) & \cos(\theta) & 0 \\ -\cos(\theta) \sin(\varphi) & -\sin(\varphi) \sin(\theta) & \cos(\varphi) \end{bmatrix} \quad (4)$$

$$\begin{bmatrix} \cos(\varphi) \cos(\theta) & -\sin(\theta) & -\cos(\theta) \sin(\varphi) \\ \cos(\varphi) \sin(\theta) & \cos(\theta) & -\sin(\varphi) \sin(\theta) \\ \sin(\varphi) & 0 & \cos(\varphi) \end{bmatrix} \quad (5)$$

Nevertheless, the definition of a number of coordinate system as large as 672 or 1170 causes a Comsol crash — likely because several hundreds of *nodes* isn't manageable by the program. For this reason, an alternative way to handle forces and constraints must be set up. Naming $X_{I_i,j}$ and $Y_{I_i,j}$, with $i = 1, 2, \dots, 4N$ and $j = 1, 2, 3$, the X and Y coordinates of P_I — the three “interface nodes” identified by the intersection of the trusses and the beams in figure 2, whose angles with respect to the actuation axis are ψ_j (ψ takes only the three values 0 and $\pm(2/3)\pi$ for $j = 1, 2, 3$) — and X_{F_i} and Y_{F_i} the X and Y coordinates of P_F — the “actuation node” of the i th actuator, identified by the intersection of the three yellow beams in figure 2 —, we can define a $4N \times 5$ matrix whose rows from i to $i + 4$ of the table are defined in (6).

$$\begin{bmatrix} X_{I_i,1} & Y_{I_i,1} & X_{F_i} & Y_{F_i} & \psi_1 \\ X_{I_i,2} & Y_{I_i,2} & X_{F_i} & Y_{F_i} & \psi_2 \\ X_{I_i,3} & Y_{I_i,3} & X_{F_i} & Y_{F_i} & \psi_3 \\ X_{F_i} & Y_{F_i} & X_{F_i} & Y_{F_i} & 0 \end{bmatrix} \quad (6)$$

The matrix defined in (6) can be easily generated in Matlab and written as a file, which can be used as table data source of the Comsol *nearest neighbor* interpolation function $\Gamma(x, y)$. Such a function, with the nodal variables $\zeta_{i,j} = X_{F_i}$, and $\eta_{i,j} = Y_{F_i}$, allow to associate to each of the three P_I coordinates the coordinates of the correspondent P_F ; moreover, Γ defines for each P_I the three angles $\Theta_{i,j} = \psi_j$. Let's define $\rho = \sqrt{\zeta^2 + \eta^2}$, $\theta' = \arctan(\eta/\zeta)$, and, similarly to (2), $\varphi' = \sum_{i=1}^{M+1} P'(i) \rho^{M+1-i}$, and substitute θ with θ' and φ with φ' in (4): the local displacement $\mathbf{u}_l = [u_l; v_l; w_l] = \mathbf{G}\mathbf{u}$, where $\mathbf{u} = [u; v; w]$ is the displacement vector in the global coordinate system, is defined in the coordinate system relative to each actuation axis. If the k th ($k = 1, 2, \dots, N$) actuator is displaced by w^* along its axis, we can define N *pointwise constraints* as in (7), in order to apply the

correct strokes to P_F , and $3N$ *pointwise constraints* as in (8) and (9), in order to radially and tangentially (in the cylindrical coordinate system of each actuator, i.e. along the red and green directions, respectively, in figure 2) restrain P_I . As a result, adding a small set of analytic function allows the computation of the N IFs avoiding any additional auxiliary coordinate system.

$$w_{l_k} = \begin{cases} 0 & \text{if } k \neq i \\ w^* & \text{if } k = i \end{cases} \quad (7)$$

$$u_{l_k} \cos(\psi_j) + v_{l_k} \sin(\psi_j) \quad j = 1, 2, 3 \quad (8)$$

$$-u_{l_k} \sin(\psi_j) + v_{l_k} \cos(\psi_j) \quad j = 1, 2, 3 \quad (9)$$

3 Results

A Matlab function, after reading the model file built by a script discussed in sections 2.1 and 2.2, runs the IF, taking the actuator number(s) as input vector and computing the forces and the displacements in the proper coordinate system.

3.1 LBT

Running the above described Matlab function gives the LBT DM 672 by 672 stiffness matrix, whose main diagonal is plotted in figure 3. An example of a single IF — the one of the actuator # 145 — is plotted in figure 4 in terms of actuator forces, while figure 5 shows the DM deformations of the portion of glass centered in the location of the actuator # 145.

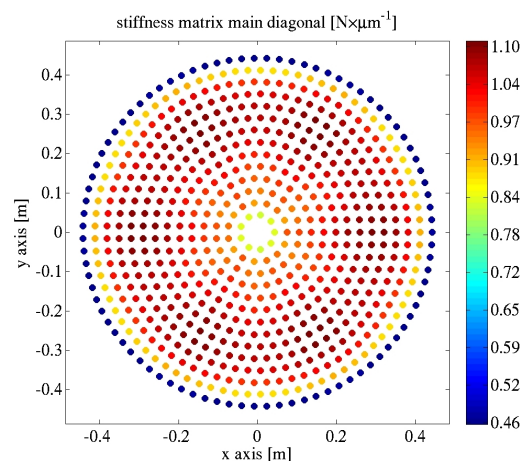


Figure 3: The main diagonal of the 672 by 672 LBT DM stiffness matrix vs. the actuator geometry.

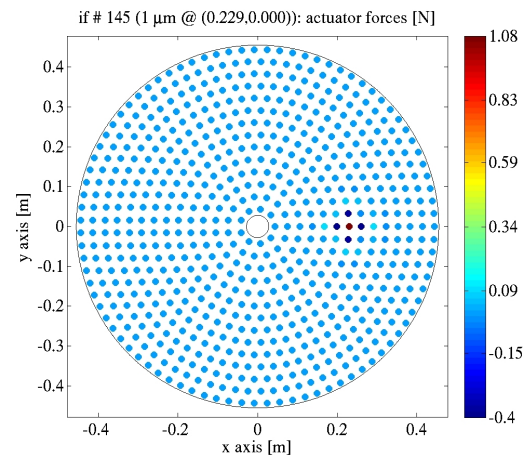


Figure 4: LBT DM: the actuator forces when the actuator #145 is displaced by $w^* = 1 \mu\text{m}$.

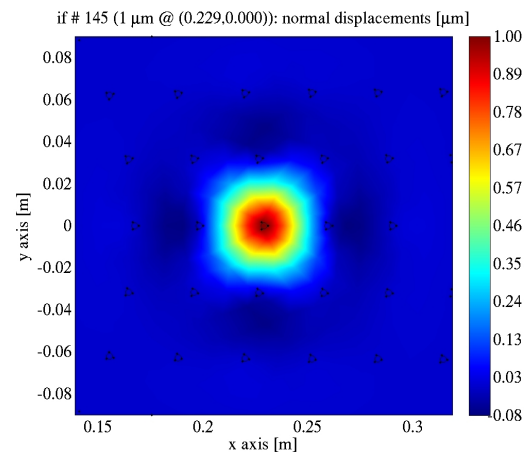


Figure 5: LBT DM: displacement normal to the surface when the actuator #145 is displaced by $w^* = 1 \mu\text{m}$.

3.2 VLT

The process described in section 3.1 gives the VLT DM 1170 by 1170 stiffness matrix, whose main diagonal is plotted in figure 6. Again, an example of a single IF — the one of the actuator # 377 — is plotted in figure 7 in terms of actuator forces, while figure 8 shows the DM deformations of the portion of glass centered in the location of the actuator # 377.

4 Experimental validation

The optical measurement of the mirror IF is part of the standard calibration procedure for deformable mirrors. As we want to compare the stiffness obtained from the FEA model with that from experimental data, we need to measure, for each IF, the actuator force applied and the actuator displacement produced.

4.1 Set-up and procedure

IFs are measured by mean of an interferometer, that provides a deformation map of the mirror using a reference Helio-Neon laser whose wavelength is 632.8 nm. The typical accuracy of an interferometer is 1 nm, over a capturing range of $\approx 40 \mu\text{m}$. During the optical test, the DM is mounted on the telescope or in a test tower and illuminated from below by the laser. Figures 9 and 10 show two IF realizations of the LBT and the VLT, respectively. In both cases, the interferometric map of a random selected actuator IF is shown over the full mirror and over a small sub-portion of it. In typical conditions, the most relevant noises affecting the measurements are convection and vibration. The vibration noise is compensated by subtracting tip and tilt from each image. The convection is reduced via a differential sampling of n frames; as a result, the typical residuals range from 1 to 5 nm RMS, to be compared with a typical actuator displacement of $\sim 100 \text{ nm}$. Such a differential sampling allows to reject constant and slowly varying terms. In order to further reduce the measurement noise, the images are collected at the fastest interferometer frame rate (25 Hz). Operatively, the procedure may be summarized as follows. Each actuator is sequentially commanded n times to the same positive and negative position, which are imaged (s_+ and s_- , respectively) by the interferometer. The resulting deformation map, $S = \frac{1}{n} \sum_{i=1}^n \frac{(s_{+i} - s_{-i})}{2}$, provides the optical shape of the actuator IF. The actuator force is measured by a current gauge installed on each actuator, whose reading is then converted into a force value via a calibration coefficient.

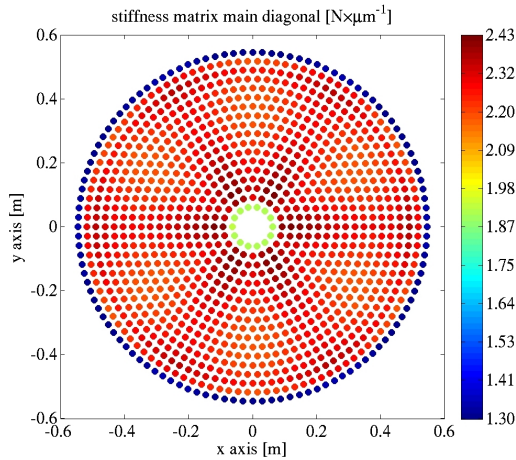


Figure 6: The main diagonal of the 1170 by 1170 VLT DM stiffness matrix vs. the actuator geometry.

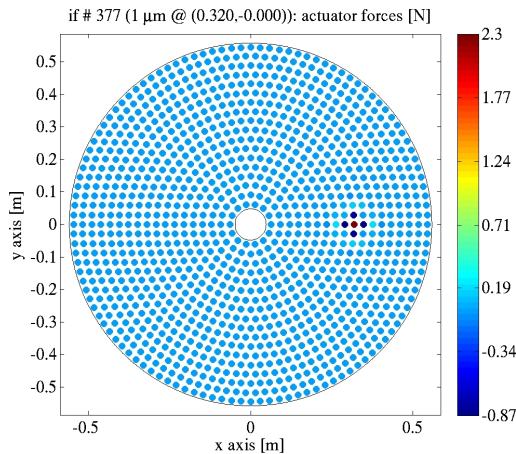


Figure 7: VLT DM: the actuator forces when the actuator #377 is displaced by $w^* = 1 \mu\text{m}$.

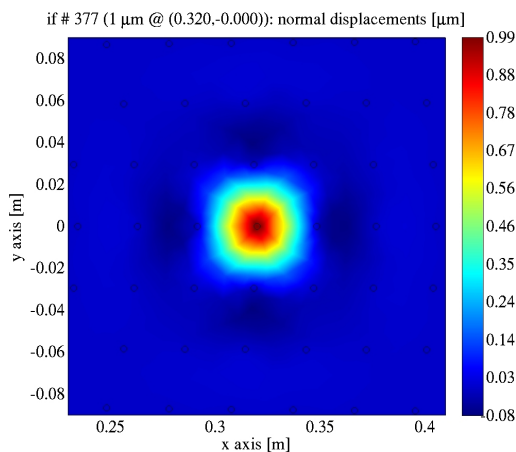


Figure 8: VLT DM: displacement normal to the surface when the actuator #377 is displaced by $w^* = 1 \mu\text{m}$.

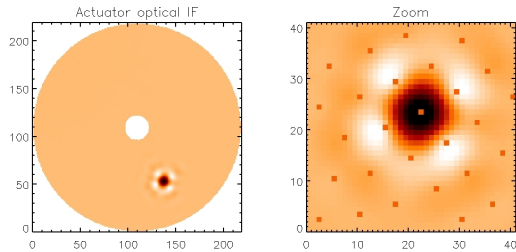


Figure 9: Example of a LBT interferometric displacement (see the text for a discussion).

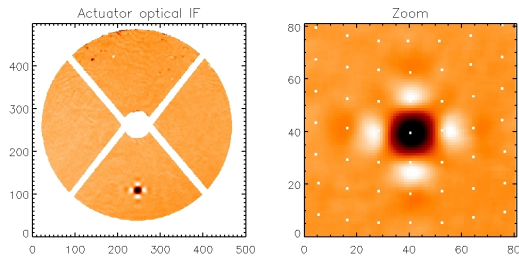


Figure 10: Example of a VLT interferometric displacement (see the text for a discussion).

4.2 Data analysis

So far, we collected the IF images and the corresponding actuator forces. The latter can be absolutely calibrated by comparing the vertical component of the DM weight with the mean force requested to keep the shell floating. However, this procedure is a *global* calibration, i.e. it is not intended to compensate actuator by actuator differences — such imprecision affects the stiffness computation. The IF images are analyzed in order to measure the actuator displacement, according to the following procedure: the location of the i th actuator is identified in the image; a mask M_{0_i} is drawn around the actuator position: the diameter of the mask is $\approx \frac{1}{5}$ of the inter-actuator distance, to enclose the peak only of the IF; the values of the pixels within M_{0_i} are averaged together, obtaining the value a_i representing the i th actuator position; a large mask M_{1_i} is drawn around the actuator position: the size is ≈ 4 times the inter-actuator distance, i.e. large enough to fully exclude the IF; the values of the pixels outside M_{1_i} are averaged together, obtaining the value r_i , that is the mirror reference position; finally, the displacement of the actuator i th is computed as $d_i = a_i - r_i$. The actuator stiffness, defined as in the FEA model, is computed as $k_i = \frac{f_i}{d_i}$.

4.3 Discussion

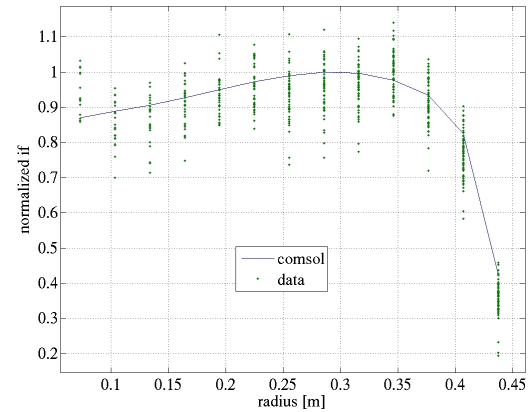


Figure 11: LBT DM IF: comparison of computed and measured data. In both cases, the IFs are normalized to their maximum value.

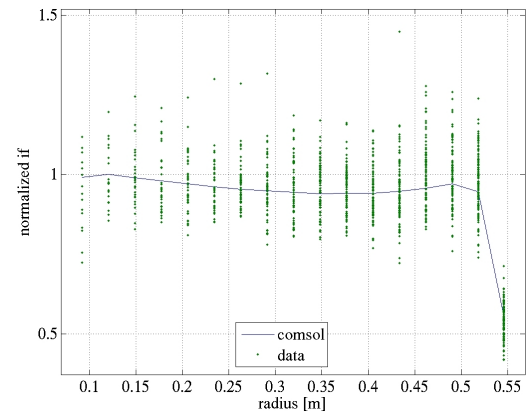


Figure 12: VLT DM IF: comparison of computed and measured data. In both case, the IFs are normalized to their maximum value.

The LBT and VLT stiffness values are plotted in figures 11 and 12, respectively, versus the actuator radial distance: as the actuators are arranged in rings, the points are accumulated in correspondence of the ring radii. The spread of the experimental stiffness values is larger than the FEA model one, because of some limitations of the sampling procedure. The most important limitations come from: actuator by actuator force calibration, relatively poor image resolution, tolerances of the actuator locations in the images, poor IF visibility for the actuators located at the edges and close to the spider arms (the hidden ones are not considered), effects of malfunctioning actuators on the surrounding ones.

5 Conclusions

Although originated by a flaw of Comsol, a *de facto* unworkability of a large number of coordinate systems, the functioning of a FEA definition as delicate as the nodal constraint reveals the powerful of the flexibility of Comsol. In fact, the availability of the Matlab computational tools allows to implement a function of the spatial coordinates able to apply the required displacements even in a complex geometry, with a compact definition of the pointwise constraints that allows a solution both fast and accurate. The precision of the results is demonstrated by the interferometric and electric measurements of the displacements and forces, respectively. In conclusion, the influence functions of an Adaptive Optics Deformable Mirror can be truthfully evaluated by the numerical method discussed in this paper — a powerful and reliable computational tool for the opto-mechanical design.

References

- [1] Roberto Biasi, Mario Andrighettoni, Gerald Angerer, Christian Mair, Dietrich Pescoller, Paolo Lazzarini, Enzo Anacleto, Marco Mantegazza, Daniele Gallieni, Elise Vernet, Robin Arsenault, Pierre-Yves Madec, Philippe Duhoux, Armando Riccardi, Marco Xompero, Runa Briguglio, Mauro Manetti, and Marco Morandini, *VLT deformable secondary mirror: integration and electromechanical tests results*, Adaptive Optics Systems III (Brent L. Ellerbroek, Enrico Marchetti, and Jean-Pierre Véran, eds.), Proc. SPIE, vol. 8447, SPIE, 7 2012.
- [2] Guido Brusa, Armando Riccardi, Valdemaro Biliotti, Ciro Del Vecchio, Piero Salinari, Paolo Stefanini, Paolo Mantegazza, Roberto Biasi, Claudio Franchini, and Daniele Gallieni, *Adaptive secondary mirror for the 6.5 conversion of the multiple mirror telescope: first laboratory testing results*, Adaptive Optics Systems and Technology (Domenico Bonaccini and Robert K. Tyson, eds.), Proc. SPIE, vol. 3762, 1999, pp. 38–49.
- [3] Ciro Del Vecchio, *Supporting a magnetically levitated, very thin meniscus for an adaptive secondary mirror: the optimization of the magnetic circuit*, Adaptive Optics and Applications (Robert K. Tyson and Robert Q. Fugate, eds.), Proc. SPIE, vol. 3126, 7 1997, pp. 605–613.
- [4] Ciro Del Vecchio, Daniele Gallieni, Hubert M. Martin, Armando Riccardi, Guido Brusa, and Roberto Biasi, *Design improvements of the LBT adaptive secondary*, Beyond Conventional Adaptive Optics (Elise Vernet, Roberto Ragazzoni, Simone Esposito, and Norbert Hubin, eds.), Proc. ESO, vol. 58, ESO, 5 2001, pp. 435–441.
- [5] Armando Riccardi, Guido Brusa, Ciro Del Vecchio, Roberto Biasi, Mario Andrighettoni, Daniele Gallieni, Fabio Zocchi, Michael Lloyd-Hart, Francois Wildi, and Hubert M. Martin, *The adaptive secondary mirror for the 6.5 m conversion of the multiple mirror telescope*, Beyond Conventional Adaptive Optics (Elise Vernet, Roberto Ragazzoni, Simone Esposito, and Norbert Hubin, eds.), Proc. ESO, vol. 58, ESO, 5 2001, pp. 55–64.
- [6] Armando Riccardi, Marco Xompero, Runa Briguglio, Fernando Quirós-Pacheco, Lorenzo Busoni, Luca Fini, Alfio Puglisi, Simone Esposito, Carmelo Arcidiacono, Enrico Pinna, Piero Ranfagni, Piero Salinari, Guido Brusa, Richard Demers, Roberto Biasi, and Daniele Gallieni, *The adaptive secondary mirror for the large binocular telescope: optical acceptance test and preliminary on-sky commissioning results*, Adaptive Optics Systems (Brent L. Ellerbroek, Michael Hart, Norbert Hubin, and Peter L. Wizinowich, eds.), Proc. SPIE, vol. 7736, SPIE, 6 2010.